Magnetic Helicity and Coronal Mass Ejections

A. Nindos

Section of Astrogeophysics, Physics Department, University of Ioannina, Ioannina GR-45110, Greece

Magnetic helicity is a quantity that descibes the chiral properties of magnetic structures. It has the unique feature that it is probably the only physical quantity which is approximately conserved even in resistive MHD. This makes magnetic helicity an ideal tool for the exploration of the physics of coronal mass ejections (CMEs). CMEs carry away from the Sun twisted magnetic fields and the concept of helicity can be used to monitor the whole history of a CME event from the emergence of twisted magnetic flux from the convective zone to the eruption and propagation of the CME into interplanetary space. I discuss the sources of the helicity shed by CMEs and the role of magnetic helicity in the initiation of CMEs.

1. INTRODUCTION

Coronal mass ejections (CMEs) are large-scale expulsions of magnetized plasma from the Sun. They are observed with a coronagraph above the occulting disk as projections on the plane of the sky. CMEs have attracted significant attention lately because they are the primary cause of the largest and most damaging space weather disturbances (e.g. Gosling 1993). In an average event, 10^{14} - 10^{16} gr of plasma is ejected into the heliosphere with speeds ranging from 100 to 2000 km/s (e.g. Howard et al. 1985; Hundhausen, Burkepile & StCyr 1994). The occurence of CMEs shows a strong solar cycle dependence: during solar minimum there is one CME every 2-3 days on average, while during solar maximum they are more frequently observed with several to more than 10 CMEs every day. CMEs sometimes, but not always, are associated with flares. Overall the occurence rate of flares is larger than the occurence rate of CMEs (averaged over a solar cycle, there are 2-3 CMEs per day while the corresponding occurence rate of GOES X-ray flares is 5-6 events per day).

Observations with a coronagraph do not reveal the correlation of CMEs with the configuration and evolution of the underlying solar structures. However, soft X-ray observations obtained with the soft X-ray telescope (SXT) on board the Yohkoh satellite and EUV observations with the EUV Imaging Telescope (EIT) on board the SOHO satellite have eased the tasks of identifying CME counterparts near the solar surface and of following the early development of the eruptions. The low corona CME counterparts (see the article by Hudson & Cliver 2001 for a detailed review) may include coronal waves, EUV and/or soft X-ray "dimmings", and long-duration soft X-ray events that occur after the CME eruption. Also SXT data reveal a relationship between coronal X-ray sigmoids and eruptivity. A flare may also destabilize an adjacent transequatorial loop structure, thus launching a CME. Note, however, that not every CME is accompanied by all the noncoronagraphic signatures listed here.

Coronagraphs observe CMEs via sunlight Thompson-scattered from free electrons and the observed signal is roughly proportional to the integrated mass along the line of sight. Nevertheless, in spite of this, the essential physics of CMEs probably resides in the magnetic field which cannot be observed directly. This argument is based on the fact that the magnetic field dominates the plasma throughout the corona because the coronal plasma $\beta << 1$ (β is the ratio of plasma to magnetic pressure). Therefore the most important forces which determine the eruption initiation and dynamics are magnetic. For the same reason, the energy required to lift the mass of a CME against gravity and accelerate it to the observed velocities is believed to be magnetic (e.g. Vourlidas et al. 2000). The fraction of magnetic energy which is converted to other forms yielding the CME initiation and motion comes from non-potential magnetic field because energy cannot be extracted from a current-free potential field. The magnetic field carried away by CMEs can be obviously helical at times. A typical example is given in Figure 1: the CME's stressed helical structure shows clearly in the bottom row of the figure. Fig. 1 also demonstrates another interesting property of the magnetic field evolution during CMEs: a part of the pre-CME magnetic configuration may contain closed field lines that open up as a result of the eruption (compare for example, the top left and the bottom right frames of fig. 1).

Figure 1

In this article, I focus on the physics of CMEs as a magnetic phenomenon. For such treatment the concept of magnetic helicity is of great importance. Magnetic helicity quantifies the chiral properties of magnetic structures and has some unique features which can help us understand several aspects of the CME physics. Note that I do not attempt to provide an exhaustive review of either CMEs or helicity; the interested reader is refered to the articles in the "Coronal Mass Ejecions" monograph (Crooker, Joselyn & Feynman 1997) and to the articles in the "Magnetic Helicity in Space and Laboratory Plasmas" monograph (Brown, Canfield, Pevtsov 1999), respectively. All I will try to do is to review the aspects of the CME phenomenon that are relevant to the concept of magnetic helicity. In section 2, the definition of magnetic helicity is given. In section 3, I discuss the sources of helicity carried away by CMEs and in section 4, I discuss what magnetic helicity can tell us about CME initiation. I present conclusions and suggestions for future work in section 5.

2. THE CONCEPT OF MAGNETIC HELICITY

2.1. Definition

Magnetic helicity is a quantity which describes nonpotential magnetic fields. For a magnetic field $\mathbf{B}$ within a volume V, it is defined as:

$$H_m = \int_V \mathbf{A}\cdot\mathbf{B}dV \tag{1}$$

where $\mathbf{A}$ is the magnetic vector potential ($\mathbf{B} = \nabla \times \mathbf{A}$). Eq. (1) is physically meaninful only when the magnetic field is fully contained inside V (i.e. at any point of the surface S surrounding V, the field's normal component B_n vanishes); this is so because the vector potential is defined through a gauge transformation ($\mathbf{A}' = \mathbf{A} + \nabla\Phi$), then H_m is gauge-invariant only when $B_n = 0$.

In the case of the solar atmosphere, magnetic flux passes through S (especially in the photosphere) and therefore the above condition is not satisfied. However, Berger & Field (1984) and Finn & Antonsen (1985) have shown that when $B_n \neq 0$ on S, we can define a gauge-invariant relative magnetic helicity H (hereafter refered to as helicity) of $\mathbf{B}$ with respect to the helicity of a reference field $\mathbf{B_p}$ having the same distribution of normal magnetic flux on the surface S surrounding V:

$$H = \int_V \mathbf{A}\cdot\mathbf{B}dV - \int_V \mathbf{A_p}\cdot\mathbf{B_p}dV \tag{2}$$

where $\mathbf{A_p}$ is the vector potential of $\mathbf{B_p}$. The quantity H does not depend on the common extension of $\mathbf{B}$ and $\mathbf{B_p}$ outside V. Being a potential field it is a convinient choice for $\mathbf{B_p}$. If in addition $\nabla\cdot\mathbf{A_p} = 0$ and $(A_p)_n = 0$ on S then the term $\int_V \mathbf{A_p}\cdot\mathbf{B_p}dV$ of eq. (2) vanishes (Berger 1988).

It is worth noting that the "natural" unit of helicity is the square of magnetic flux (Mx^2) and therefore the helicity of a twisted flux tube with N turns and magnetic flux equal to unity is simply N. For more complex magnetic topologies, helicity can be regarded as a measure of the topological complexity of the magnetic field (e.g. linkage and twistedness in the field).

2.2. Flux of Magnetic Helicity

Generally, the amount of helicity within V can change either due to helicity flux crossing S or/and due to dissipation within V. Berger (1984) has demonstrated that the helicity dissipation rate is negligible in all processes taking place in the corona, including reconnection and all non-ideal processes. Helicity's dissipation time scale is the global diffusion time scale. As an example, I note that Berger (1984) found that the minimum helicity dissipation time in a typical coronal loop is about 10^5 years. Consequently, helicity can be regarded as an (almost) conserved quantity even in resistive MHD. The fact that it is one of the few (probably the only) quantities that it is preserved in the absence or near absence of resistivity makes it a powerful tool that can help us trace the transport of magnetic field from the subphotospheric layers to the corona, and then its ejection into the interplanetary medium.

For convenience, the temporal evolution of helicity across the photospheric boundary S_p can be separated into a tangential term $dH/dt|_t$ and a normal term $dH/dt|_n$. Then according to Berger (1999) we get

$$\frac{dH}{dt}\bigg|_t = -2\oint(\mathbf{v_t}\cdot\mathbf{A_p})B_n dS_p \tag{3}$$

$$\frac{dH}{dt}\bigg|_n = 2\oint(\mathbf{A_p}\cdot\mathbf{B_t})v_n dS_p \tag{4}$$

where B_t and B_n are the tangential and normal components of the magnetic field on the photosphere and $\mathbf{v_t}$ and $\mathbf{v_n}$ the tangential and normal components of the photospheric plasma velocity. Eq. (3) gives the change of helicity due to horizontal motions on the photospheric surface. Such motions may come either from differential rotation and/or from transient photospheric shearing flows. Eq. (4) gives the change of helicity due to the emergence of twisted field lines that cross the photosphere.

3. The Sources of Helicity Carried Away by CMEs

3.1. CMEs as a Way of Removing Helicity from the Corona

The solar cycle dependence of the CME occurence rate may imply that CMEs are somehow connected to the solar dynamo. Over the years, it has been realized that in several occasions magnetic fields emerging from the solar interior to the photosphere are twisted (e.g. Leka et al. 1996, Zhang 2001). This indicates that a significant fraction of active region's helicity is created by the dynamo and then transported into the corona through the photosphere with the emerging magnetic flux. Since helicity is not destroyed under reconnection (see section 2.2) this process accumulates helicity in the corona. Furthermore, on the global scale, helicity emerges predominantly negative in the northern hemisphere and predominantly positive in the southern hemisphere (Seehafer 1990, Pevtsov, Canfield, & Metcalf 1995). And also this hemispheric helicity sign pattern does not change from solar cycle to solar cycle (Pevtsov, Canfield, & Latushko 2001). Consequently, on the global scale, mutual cancellation of helicity of opposite signs cannot relieve the Sun from excess accumulated helicity. It has been suggested (e.g. Low 1996) that CMEs, as expulsions of twisted magnetic fields, consist an important process through which accumulated helicity is removed from the corona.

The above statement is supported from solar wind observations. In situ magnetic field measurements show that there are sporadic intervals when magnetic fields are twisted in either a right-handed or left-handed sense, corresponding to positive and negative helicity, respectively. Such disturbances are called magnetic clouds (MCs) when they show enhanced magnetic field whose vector direction rotates gradually through 180°. MCs have been often associated with disappearing filaments on the Sun (e.g. Marubashi 1986; Rust 1999) and have been interpreted as magnetic flux ropes ejected from the corona as CMEs. Consequently, MCs can be regarded as the interplanetary manifestations of some CMEs (note, however, that not all CMEs give MCs at 1 AU). The observations show (Rust 1994, Bothmer & Schwenn 1994) that the number of MCs with positive chirality (i.e. handedness) is roughly equal to the number of MCs with negative chirality. But CMEs that originate from the northern hemisphere tend strongly to have negative chirality in the corresponding MCs, and those from the southern hemisphere have positive chirality in their MCs.

3.2. The Helicity Budget of CME-Productive Active Regions

Once it was realized that CMEs remove helicity from the corona, the obvious question was where that helicity comes from. In section 2.2, I mentioned that on the photospheric surface, helicity may change either due to shearing horizontal motions or/and due to the emergence of twisted field lines that cross the photosphere. For the computation of the helicity budget of an active region, one needs to compute the helicity injection rate from eq. (3) and (4) and also the helicity stored in the corona and the helicity ejected into interplanetary space.

The first process which was studied was differential rotation (DeVore 2000). Démoulin et al. (2002a) and Green et al. (2002) studied the long-term evolution of the helicity injected by differential rotation into the coronal part of two active regions which were followed from their birth until they decayed. The helicity injection rate from differential rotation was calculated as the sum of the rotation rate of all pairs of elementary fluxes weighted with their magnetic flux. The coronal magnetic field was modeled under the force-free field assumption ($\nabla \times \mathbf{B} = \alpha \mathbf{B}$, e.g. see Alissandrakis 1981). The best value of α, α_{best}, is determined by comparing the computed field lines with the observed soft X-ray or EUV coronal structures. Then the computation of the coronal helicity is relatively straightforward (Berger 1985). The helicity carried away by CMEs cannot be directly computed. In order to overcome this problem one assumes that each CME ejected from the active region under study produces a MC, and that the helicity carried away by each CME is equal to the helicity in the corresponding MC. The helicity per unit of length in a MC can be calculated if we know the axial magnetic field B_0 and the radius R of the cloud's flux rope (DeVore 2000). These parameters can be calculated using a magnetic field model (Lepping, Burlaga, & Jones 1990) that assumes that the magnetic field's twist along the interplanetary flux tube is uniform and the field within the MC is described by the first harmonic of a linear force-free field. For the calculation of the total MC helicity, the cloud's flux tube axis ℓ is needed which cannot be obtained observationally; usually a lower limit of $\ell = 0.5$ AU and an upper limit of $\ell = 2$ AU are used. Démoulin et al. (2002a) and Green et al. (2002) found that the helicity injected by differential rotation is at least about an order of magnitude smaller than the helicity stored in the corona and the helicity carried away by CMEs.

When high-cadence photospheric longitudinal magnetograms are available, the horizontal velocity appearing in eq. (3) can be computed using the local correlation tracking (LCT) technique (November & Simon 1988). Several authors have computed the corresponding helicity injection rate (Chae 2001, Nindos & Zhang 2002, Moon et al. 2002a,b, Nindos, Zhang, & Zhang 2003, Chae et al. 2004). However, as Démoulin & Berger (2003) have pointed out, with the magnetograms one follows the photospheric intersection of the magnetic flux tubes but not the evolution of the plasma (generally the two velocities are different). Consequently, from the observed magnetic evolution we obtain the flux tube motion and not the plasma motion parallel to the photosphere. If v_t is the tangential component of the photospheric plasma velocity and v_n the velocity perpendicular to the photosphere, the LCT method detects the velocity of the footpoints of the flux tube which is

$$\mathbf{u} = \mathbf{v_t} - \frac{v_n}{B_n}\mathbf{B_t} \tag{5}$$

If we insert this expression for the velocity in eq. (3) we get the whole helicity flux density (see eqs [3] and [4]). Consequently, one may use the quantity $G = -2\mathbf{u}\cdot\mathbf{A_p}B_n$ as a proxy to the helicity flux density. Recently, Pariat et al. (2005) have proposed a different proxy to the helicity flux density. Its concept is based on the fact that the helicity injection rate can be understood as the summation of the rotation rate of all pairs of elementary fluxes weighted with their magnetic flux (Berger 1984). The resulting quantity can be derived from observations but such calculations have not been done yet.

A typical sequence of computed velocity vectors and the corresponding maps of G is given in Figure 2. The velocity vectors reflect mainly two large-scale systematic flow patterns: (1) a radial outflow of moving magnetic features from the sunspot's moat and (2) the initially westward and then

Figure 2

northwestward motion of the whole sunspot. A purely westward motion of a symmetric sunspot gives no net helicity injection because G has opposite sign contribution in its northern and southern part (see the bipolar structure of G above the sunspot). The bulk of the net helicity injection in AR 8375 comes from deviations from such situation (shearing and twisting components of the motions of the sunspot and moving magnetic features with respect to opposite flux concentrations, polarity deformations and asymmetries in B_n repartition). Despite the spatial incoherence of the computed G maps, Nindos et al. (2003) were able to partially reconcile the amount of helicity injected into the corona with the helicity carried away by the CMEs in the 6 six active regions they studied. When they assumed that the length of the MC's flux tube ℓ is determined by the condition for the initiation of the kink instability in the coronal flux rope or $\ell = 0.5$ AU then the total CME helicities and the total helicities injected into the corona were broadly consistent. However, for $\ell = 2$ AU, the total helicities injected into the corona were a factor of 2.9-4 lower than the total CME helicities.

It is important to note that the LCT method has serious limitations that lead to underestimation of the computed helicities (Démoulin & Berger 2003). Furthermore, the method described above, cannot separate the contribution of the shearing term (eq. 3) from the contribution of the advection term (eq. 4) to the helicity injected into the corona. The theoretical work by Démoulin et al. (2002b) who separated the helicity injection into two terms, twist and writhe, indicates that shearing motion is an inefficient way of providing helicity on the active region scale which will be subsequently removed by CMEs. Recently, alternative approaches have been developed which attempt to compute separately both the shearing and advection term using photospheric vector magnetograms. Kusano et al. (2002) proposed a method which uses the vertical component of the induction equation. In fact the velocity of flux tubes cannot be deduced fully from the induction equation and part of the velocity is still computed from the LCT method (Welsch et al. 2004). When the transverse component of the magnetic field is available, Kusano et al. (2004) developed a method which minimizes the input from the LCT technique. Longcope (2004) introduced a technique which demands that the photospheric flow agree with the observed photospheric field evolution according to the magnetic induction equation. It selects, from all consistent flows, that with the smallest overall flow speed by demanding that it minimize an energy functional. Georgoulis & LaBonte (2005) introduce a minimum structure reconstruction technique to infer the velocity field vector. Their analysis simultaneously determines the field-aligned flows and enforces a unique cross-field velocity solution of the induction equation. All these methods have not been tested extensively with data. Also the comparison of their results when applied to the same set of simulated data shows differences (Georgoulis, private communication).

4. Magnetic Helicity and CME Initiation

CMEs carry away coronal plasma and open up magnetic field lines which were closed before the eruption. Therefore, the pre-eruption state must contain enough magnetic energy to account for the observed gravitational potential and kinetic energies of the CMEs and also the energy required to open up the magnetic field. The latter imposes a difficulty to all CMEs models that comes from the Aly-Sturrock theorem (Aly 1991, Sturrock 1991). This theorem establishes that in the case of an open field in which all of the field lines extend to infinity, the magnetic energy increases during the eruption. Consequently, one needs a process capable of opening the field and at the same time decrease its energy by the amount required to power the mass motion. However, as Forbes (2000) has summarized, there are several ways to bypass this constraint: (1) the CME involves flux from several flux systems so most of the field involved is not opened (Antiochos, DeVore, & Klimchuk 1999), (2) the CME involves a detached flux rope (Low 1996), (3) an ideal MHD process may extend field lines such that they do not open all the way to infinity, (4) the pre-CME corona is not force-free and cross-field currents are present (Wolfson & Dlamini 1997), (5) non-ideal processes, specifically reconnection, might be important.

The processes leading to CMEs require helicity accumulation to the magnetic structure that will subsequently erupt. This can be done by shearing the magnetic field or by assuming a pre-existing flux rope. Several mechanisms are capable of shearing the pre-eruption field: emergence of twisted flux, shearing, twisting, and convering motions (the fact that the large amount of shear applied to several models is not observed in the photosphere poses a problem in our understanding of CME initiation). Then the eruption can be regarded as a failure of field confinement. Overall, the current status of our understanding of CME initiation gives a very important role to magnetic helicity and reconnection. In order to appreciate fully the role of helicity in the initiation of CMEs we discuss in the next subsection two important theoretical arguments.

4.1. Woltjer Theorem and Taylor Relaxation

Woltjer (1958) showed that for a perfectly conducting plasma, the total magnetic helicity remains invariant during the evolution of any closed flux system and the minimum energy state of this system corresponds to a linear force-free field configuration. This statement has been proved mathematically and is known as Woltjer theorem. Taylor (1974) applied that theorem to the subject of plasma relaxation by proposing that turbulent magnetic reconnection will occur in a plasma of small but finite resistivity to change field topology and transport helicity from one part of the plasma to another, until the field reaches its minimum energy state which is the linear force-free configuration, according to Woltjer theorem. Therefore, while in the limiting case of ideal MHD the helicity of each field line will be an invariant of motion, Taylor's conjecture suggests that only the total helicity of the flux system will be approximately invariant during its evolution to the minimum energy state. A way to understand Taylor's theory is that the magnetic energy should be selectively dissipated faster than the magnetic helicity and that the final state of the linear force-free field might be self-organized.

The relevance of Taylor's theory to solar plasmas is still under debate. While some 3D numerical MHD simulations of relaxation processes in the corona indeed show such a relaxation toward a constant α-field (Kusano et al. 1994), other simulations (Amari & Luciani 2000, Antiochos & DeVore 1999) show a more complicated behavior at variance with Taylor's theory. Antiochos & DeVore (1999) have argued that Taylor's theory requirement that complete reconnection occurs, i.e. reconnection continues until magnetic energy reaches its lowest possible state, is wrong because complete reconnection requires the formation of numerous current sheets that do not form easily in the corona due to photospheric line-tying. However, Nandy et al. (2003) report the detection of a Taylor-like plasma relaxation process in the corona: their statistical study of highly flare-productive active regions implies that the magnetic field relaxes toward a constant-α configuration.

4.2. The Hydromagnetic Origin of CMEs

Low and Zhang in a series of papers (Low 1996, 1999, Low & Zhang 2002, Zhang & Low 2001, 2003) provided a unified theoretical view of CMEs as the last physical mechanism in the chain of processes that transfer magnetic flux and helicity from the base of the convective zone into the interplanetary medium. In this section I summarize their results with emphasis on the role of helicity in the initiation of CMEs. New active regions emerge with twisted magnetic field and magnetic polarities opposite to that of the pre-existing field. When the new field enters the corona, repeated reconnections between the new and pre-existing field take place. This process simplifies the magnetic topology and the dissipated magnetic energy produces flares. Finally the field achieves its minimum-energy state which is the constant-α force-free configuration required by the Woltjer-Taylor theories. An example of such process is given in Figure 3 taken by Zhang & Low (2003). The left panel of fig. 3 shows the initial state of a current-sheet field whose interface (i.e. the

Figure 3

current sheet denoted by the thick solid line) separates two axisymmetric force-free fields. The final minimum-energy state of the field resulting from Taylor relaxation is given in the right panel of fig. 3. Note that the relaxation resulted in the formation of a flux rope: the redistribution of helicity, whose total amount is conserved, yields a minimum-energy state where a significant part of the total helicity of the system is contained within the flux rope.

The fate of the flux rope is determined by the efficiency of its confinement by its surrounding anchored field. Flux rope ejection occurs when the magnetic energy it contains is sufficient to drive an outward expansion against the confining field. MHD simulations by Zhang, Stone, & Low (2003) explored the conditions required for the failure of confinement of a flux rope. Their work shows that the ratio of the emerging flux to the preexisting flux determines the dynamics of the flux rope: if this ratio is below a critical value, the flux rope remains in a quiescent state in the corona. But if the ratio of the emerging flux to the pre-existing flux is high then the flux rope escapes from the computational box.

We may generalize the above findings as follows. Reconnection liberates magnetic energy by changing the field topology, but not all the magnetic free energy can be so released due to the conservation of the total helicity. Therefore, so long as a magnetic structure is confined to the corona during its relaxation through reconnection and its total helicity is significant, its relaxed state is a twisted field that conserves that total helicity. Trapped with that total helicity is a fraction of the magnetic free energy that cannot be released by reconnection. The removal of the trapped helicity and magnetic energy is achieved by the bodily expulsion of the twisted structure, i.e. the CME (Low 1994, 1996).

The physical view by Low and Zhang presented in this subsection is supported by the work by Nindos & Andrews (2004). The starting point of their work was the study by Andrews (2003) who found that approximately 40% of M-class flares between 1996 and 1999 are not associated with CMEs. Nindos & Andrews (2004) modeled under the constant α force-free field approximation, the pre-flare coronal magnetic field of 78 active regions from Andrews's (2003) data set. Then from the derived values of α_{best} (see §3.2 for its definition), they computed the corresponding coronal helicites H_c. Their results appear in Figure 4 and Figure 5. In both figures, both the scatter plots and histograms show clearly that several ARs that give big flares without CMEs tend to have smaller absolute values of α_{best} and H_c than those producing CME-associated flares. They found that this result is statistically significant: their analysis demonstrated that in a statistical sense, both the preflare absolute value of α and the corresponding coronal helicity of the active regions producing CME-associated big flares are larger than

Figure 4

Figure 5

the absolute α and coronal helicity of those that do not have associated CMEs. The study by Nindos & Andrews (2004) indicates that the amount of the preflare stored coronal helicity may determine whether a big flare will be associated with a CME or not.

In this section the Low and Zhang unified picture of CMEs as an hydromagnetic phenomenon was summarized. However,the consequences of the helicity conservation and Taylor relaxation have been applied to oversimplified magnetic configurations. More realistic magnetic topologies may reveal new aspects and/or modify the picture. Furthermore, the analysis of observations may reveal new results and supply the modeling efforts with valuable input.

4.3. Other approaches

Several other approaches to the problem of CME initiation have appeared in the literature. The purpose of this article is not to present an exhaustive review of all CME models; the interested reader may refer to the excellent articles by Forbes (2000) and Klimchuk (2001). Here I focus on the role of helicity in selected representative CME models. Overall, in most models the initiation of a CME comes from the interplay between the accumulation of helicity into the corona and reconnection. In most models the pre-eruption topology is either a sheared arcade (bipolar or quadrupolar configuration) or a flux rope. It has been suggested that in CMEs showing the "three-part structure" (i.e. a bright frontal loop, a dark cavity underneath, and an embedded bright core), cavities correspond to flux ropes seen edge-on. However, not all CMEs have a clear three-part structure. Additional evidence of the flux rope topology in some events is the in situ observation of a rotating magnetic field pattern in magnetic clouds. In §4.2, we discussed that in the framework of Taylor relaxation, flux ropes may be regarded as the inevitable outcome in a structure with sufficient accumulation of helicity. But the observation of a flux rope in a CME does not necessarily suggest that the flux rope was part of the initial configuration because reconnection may cause flux ropes to form from erupting sheared arcades (Gosling 1990).

Antiochos, DeVore, & Klimchuk (1999) developed the "breakout model" which follows the evolution of a quadrupolar magnetic field in which the inner part of the central arcade is sheared by antiparallel footpoint motions near the neutral line. As a result, reconnection between the sheared field and its neighboring field triggers an eruption. Reconnection removes the overlying unsheared field to allow the low-lying sheared field to open up. MacNeice et al. (2004) have studied the evolution of helicity under the breakout model (see Plate 1). In their simulation, the model has been driven by a shear flow that injects both free energy and net helicity into the corona. Their results show that the helicity Plate 1 shed by the plasmoid ejection is at least 80% of the total originally injected into the system. They interpreted this result as an indication that although CMEs remove the bulk of the coronal helicity, some fraction remains behind (in the bottom row of Plate 1, this is indicated by the red color appearing in the closed field corona after the plasmoid's ejection). MacNeice et al. (2004) suggest that some other mechanism (possibly small-scale diffusion) might be responsible for dissipating the rest of the helicity. Furthermore, Phillips et al. (2005) presented simulations of the breakout model where eruption occurs even when no net helicity is injected into the corona. In their simulations the eruption occurs at a fixed magnitude of free energy in the corona, independent of the value of helicity. It would be desirable to check these results against computations of the helicity evolution in observed eruptions that appear to be due to breakout.

Amari et al. (2003a, 2003b) have constructed a set of force-free fields having different magnetic flux and helicity contents and used them as initial conditions by applying converging motions or a diffusion-driven evolution. These processes can trigger eruptive events that may be either confined or unconfined, depending on the value of the initial helicity. Amari et al. (2003b) concluded that the helicity cannot be the only parameter controlling the triggering of an ejection: having a large enough helicity seems a necessary condition for an ejection to occur, but not a sufficient one.

Other CME models include the catastrophe model developed by Forbes and colleagues (e.g. Forbes 1990, Lin, Forbes, & Isenberg 2001) where the CME comes from a catastrophic loss of equilibrium. In the model by Wu et al. (1999) the CME is produced from the interaction between a pre-existing flux rope and the overlying helmet streamer. In the model by Linker & Mikic (1995), the CME initiation requires reconnection at the base of a sheared arcade. The model by Chen (1996) involves an equilibrium flux rope which contains a low-density hot component and a denser cold component. The eruption of the entire flux rope is triggered by an increase in the azimuthal magnetic flux of the structure.

5. Conclusions and Future Work

Magnetic helicity provides an important tool for the study of CME physics. Its use is justified by two key properties of CMEs: (1) the pre-eruption magnetic topology is non-potential (either a sheared arcade or flux rope) and (2) CMEs carry away twisted magnetic fields. Of course, there are also other physical quantities that describe non-potential fields, for example the α parameter of the force-free field approximation. But helicity is superior because of its unique feature of being conserved even in resistive MHD on time-scales less than the global diffusion time-scale. This makes helicity probably the only physical quantity which can monitor the entire history of the event: from the transfer of magnetic field from the convective zone all the way to the eruption and the escape of the CME into the interplanetary medium. On the other hand, the calculations of helicity are difficult and only recently attempts have been made to measure helicity using solar observations.

Once the importance of helicity was realized, a lot of effort was put on the helicity budget of CME-productive active regions and on the mechanisms which provide the helicity shed by CMEs. Theoretical considerations have demonstrated rigorously that shearing motions (either differential rotation and/or transient flows) on the photospheric surface is an inefficient way of providing helicity on the active region scale. However, computations using high-cadence longitudinal magnetograms give the total helicity flux and cannot separate the shearing term from the advection term. Furthermore, the computation of velocities using the LCT method has serious limitations. Attempts for the computation of the shearing and advection term separately have been made using vector magnetograms. But the algorithms that have been developed have not been applied extensively to observations. Even more serious uncertainties are associated with the computation of the helicity carried away by the CMEs. The use of MCs as proxies for the calculation of CME helicity is only a zero-order approximation. All the above problems contribute to the discrepancies concerning the helicity budget of active regions. At this point, these uncertainties have been cleared up only partially and much work needs to be done on this issue.

The new generation of ground-based and space-born vector magnetograms (e.g. SOLIS and the instruments on board the coming "Solar B" and SDO missions) will provide important new data that should trigger the development of improved algoriths for the computation of the helicity injected into the solar atmosphere. Concerning the helicity of magnetic clouds, we need to constrain more accurately the length of magnetic cloud flux tubes and investigate whether the twist along the interplanetary flux tube is uniform. Hopefully, the coming STEREO mission will provide important observational input to such tasks.

The role of helicity in the initiation of CMEs is a theoretical subject of intense debate. There is a general consensus that for the CME initiation, helicity must be accumulated to the pre-eruption topology. However, diverse opinions exist about the importance of helicity in the overall coronal evolution which leads to a CME. It has been argued that conservation of global helicity plays a minor role in determining the nature and consequences of reconnection in the Sun. The basic argument that supports this point of view is that the coronal magnetic field violates Taylor-theory's requirement that reconnection continues until the magnetic energy reaches its lowest possible state.

Helicity is a crucial element in the other approach which views CMEs as the last chain of a unified process that starts with emergence of twisted magnetic flux from the sub-photospheric layers. This point of view exploits the conservation of total helicity and accepts that magnetic energy should be selectively dissipated faster than magnetic helicity; it takes these arguments to their full logical conclusions and implications. Flux emergence charges the corona with helicity and the excess magnetic energy is removed by reconnection events (i.e. flares). But not all the magnetic energy can be so released due to the conservation of total helicity. The relaxed state is a twisted structure that conserves the total helicity. The CME is the removal of the trapped helicity, enabling the field to reach its minimum-energy state. Recent results from observations give indirect support to that picture. On the theoretical front, the picture should be refined using more realistic magnetic topologies. Observationally, it will be desirable to test whether there is a helicity threshold above which the accumulated helicity results to CME initiation.

Acknowledgments. I thank the organizers of the AGU Chapman Meeting for inviting me to give this review. I also thank M. Georgoulis for his useful comments on the manuscript. Thanks are also due to C.E. Alissandrakis, P. Démoulin, H. Zhang, J. Zhang, S.K. Antiochos, D. Rust and N. Gopalswamy for useful discussions and/or help.

REFERENCES

Alissandrakis, C.E., On the computation of constant alpha force-free magnetic field, A&A, 100, 197-200, 1981

Aly, J.J., How much energy can be stored in a three-dimensional force-free magnetic field?, ApJ (Lett), 375, L61-64, 1991.

Amari, T., and J.F. Luciani, Helicity redistribution during relaxation of astrophysical plasmas, Phys. Rev. Lett., 84, 1196-1199, 2000.

Amari, T., J.F. Luciani, J.J. Aly, Z. Mikic, and J. Linker, Coronal mass ejection: initiation, magnetic helicity, and flux ropes: II. boundary motion-driven evolution, ApJ, 585, 1073-1086, 2003a.

Amari, T., J.F. Luciani, J.J. Aly, Z. Mikic, and J. Linker, Coronal mass ejection: initiation, magnetic helicity, and flux ropes: II. Turbulent diffusion-driven evolution, ApJ, 595, 1231-1250, 2003b.

Andrews, M.D., A search for CMEs associated with big flares, Sol. Phys., 218, 261-279, 2003.

Antiochos, S.K., and C.R. DeVore, The role of helicity in magnetic reconnection: 3D numerical simulations, in *Physics of Magnetic Flux Ropes, Geophys. Monogr. Ser.*, vol. 111, edited by M.R. Brown, R.C. Canfield, and A.A. Pevtsov, pp. 187-196, AGU, Washington DC, 1999.

Antiochos, S.K., C.R. DeVore, and J.A. Klimchuk, A model for solar coronal mass ejections, ApJ, 510, 485-493, 1999.

Berger, M.A., Magnetic helicity in the solar corona, PhD thesis, Harvard University, Cambridge MA., 1984.

Berger, M.A., Structure and stability of constant-alpha force-free fields, ApJ (Suppl.), 59, 433-444, 1985.

Berger, M.A., An energy formula for nonlinear force-free magnetic fields, A&A, 201, 355-361, 1988.

Berger, M.A., Magnetic helicity in space physics, in *Physics of Magnetic Flux Ropes, Geophys. Monogr. Ser.*, vol. 111, edited by M.R. Brown, R.C. Canfield, and A.A. Pevtsov, pp. 1-9, AGU, Washington DC, 1999.

Berger, M.A., and G.B. Field, The topological properties of magnetic helicity, Journal of Fluid Mech., 147, 133-148, 1984.

Bothmer, V., and Schwenn, R., Eruptive prominences as sources of magnetic clouds in the solar wind, Space Sci. Rev., 70, 215, 1994.

Brown, M.R., R.C. Canfield, A.A. Pevtsov (Eds.), *Helicity in Space and Laboratory Plasmas,*, 304 pp., Geophys. Monogr. Ser., vol. 111, AGU, Washington DC, 1999

Chae, J., Observational determination of the rate of magnetic helicity transport through the solar surface via the horizontal motion of field line footpoints, ApJ, 560, L95-98, 2001.

Chae, J., Y.-J. Moon, and Y.-D. Park, Determination of magnetic helicity content of soalr active regions from SOHO/MDI magnetograms, Sol. Phys., 223, 39-55, 2004.

Chen, J., Theory of prominence eruption and propagation: interplanetary consequences, JGR, 101, 27499-27520, 1996.

Crooker, N., J.A. Joselyn, and J. Feynman (Eds.), *Coronal Mass Ejections,* 299 pp., Geophys. Monogr. Ser. vol. 99, AGU, Washington DC, 1997.

Démoulin, P., and M.A. Berger, Magnetic energy and helicity fluxes at the photospheric level, Sol. Phys., 215, 203-215, 2003.

Démoulin, P., C.H. Mandrini, L. van Driel-Gesztelyi, B.J. Thompson, S. Plunkett, Zs. Kovari, G. Aulanier, and A. Young, What is the source of the magnetic helicity shed by CMEs? The long-term helicity budget of AR 7978, A&A, 382, 650-665, 2002a

Démoulin, P., C.H. Mandrini, L. van Driel-Gesztelyi, M.C. Lopez Fuentes, and G. Aulanier, The magnetic helicity injected by shearing motions, Sol. Phys., 207, 87-110, 2002b

DeVore, C.R., Magnetic helicity generation by solar differential rotation, ApJ, 539, 944-953, 2000.

Georgoulis, M.K., and B.J. LaBonte, Reconstruction of inductive velocity field vector from doppler motions and a pair of solar vector magnetograms, ApJ, submitted, 2004.

Gosling, J.T., The solar flare myth, JGR, 98, 18, 18937-18949, 1993a

Finn, J.H., and T.M. Antonsen, Magnetic helicity: what is it, and what is it good for?, *Comments on Plasma Phys. and Contr. Fusion*, 9, 111, 1985.

Forbes, T.G., Numerical simulation of a catastrophe model for coronal mass ejections, JGR, 95, 11919-11931, 1990.

Forbes, T.G., A review on the genesis of coronal mass ejections, JGR, 105, 23153-23165, 2000.

Gosling, J.T., Coronal mass ejections and magnetic flux ropes in interplanetary space, in *Physics of Magnetic Flux Ropes, Geophys. Monogr. Ser.*, vol. 58, edited by C.T. Russell, E.R. Priest, and L.C. Lee, pp. 343-364, AGU, Washington DC, 1990.

Gosling, J.T., The solar flare myth, JGR, 98, 18, 18937-18949, 1993.

Green, L.M., M.C. Lopez-Fuentes, C.H. Mandrini, P. Démoulin, L. van Driel-Gesztelyi, and J.L. Culhane, The magnetic helicity budget of a CME-prolific active region, Sol. Phys., 208, 43-68, 2002.

Howard, R.A., N.R. Sheeley, Jr, M.J. Koomen, and D.J. Michels, Coronal mass ejections 1979-1981, JGR, 90, 8173-8191, 1985.

Hudson, H.S., and E.W. Cliver, Observing coronal mass ejections without coronagraphs, JGR, 106, 25199-25213, 2001.

Hundhausen, A.J., J.T. Burkepile, and O.C. St. Cyr, Speeds of coronal mass ejections: SMM observations from 1980 and 1984-1989, JGR, 99,6543-6552

Klimchuk, J.A., Theory of coronal mass ejections, in *Space Weather, Geophys. Monogr. Ser.*, vol. 125, edited by P. Song, H.J. Singer, and G.L. Siscoe, pp. 143-158, AGU, Washington DC, 2001.

Kusano, K., Y. Suzuki, H. Kubo, T. Miyoshi, and K. Nishikawa,Three-dimensional simulation study of the magnetohydrodynamic relaxation process in the solar corona. 1: Spontaneous generation of Taylor-Heyvaerts-Priest state, ApJ, 433, 361-378 1994.

Kusano, K., T. Maeshiro, T. Yokoyama, and T. Sakurai, Measurement of magnetic helicity injection and free energy loading into the colar corona, ApJ, 577, 501-512, 2002.

Kusano, K., T. Maeshiro, T. Yokoyama, and T. Sakurai, in ASP Conference Series, in press.

Leka, K.D., R.C. Canfield, A.N. McClymont, and L. van Driel-Gesztelyi, Evidence for current-carrying emerging flux, ApJ, 462, 547-560, 1996.

Lepping, R.P., L.F. Burlaga, J.A. Jones, Magnetic field structure of interplanetary magnetic clouds at 1 AU, JGR, 95, 11957-11965, 1990.

Lin, J., T.G. Forbes, P.A. Isenberg, Prominence eruptions and coronal mass ejections triggered by newly emerging flux, JGR, 106, 25053-25074, 2001.

Linker, J.A., and Z. Mikic, Disruption of a helmet streamer by photospheric shear, ApJ, 438, L45-L48, 1995.

Longcope, D.W., Inferring a photospheric velocity field from a sequence of vector magnetograms: the minimum energy fit, ApJ, 612, 1181-1192, 2004

Low, B.C., Magnetohydrodynamic processes in the solar corona: flares, coronal mass ejections, and magnetic helicity, Phys. Plasmas, 1, 1684-1690, 1994.

Low, B.C., Solar activity and the corona, Sol. Phys., 167, 217-265, 1996.

Low, B.C., and M. Zhang, The hydromagnetic origin of the two dynamical types of solar coronal mass ejections, ApJ, 564, L53-56, 2002.

MacNeice, P., S.K. Antiochos, A. Phililips, D.S. Spicer, C.R. DeVore, and K. Olson, A numerical study of the breakout model for coronal mass ejection initiation, ApJ, 614, 1028-1041.

Marubashi, K., Structure of the interplanetary magnetic clouds and their solar origins, Adv. Space Res., 6, 335-338, 1986.

Moon, Y.-J., J. Chae, H. Wang, G.S. Choe, Y.D. Park, Impulsive variations of the magnetic helicity change rate associated with eruptive flares, ApJ, 580, 528-537, 2002a.

Moon, Y.-J., et al., Flare activity and magnetic helicity injection by photospheric horizontal motions, ApJ, 574, 1066-1073, 2002b.

Nandy,D., M. Hahn, R.C. Canfield, and D.W. Longcope, Detection of a Taylor-like plasma relaxation process in the Sun, ApJ, 597, L73-L76, 2003.

Nindos, A., and H. Zhang, Photospheric motions and coronal mass ejection productivity, ApJ, 573, L133-136, 2002.

Nindos, A., and M.D. Andrews, The association of big flares and coronal mass ejections: what is the role of magnetic helicity?, ApJ, 616, L175-178, 2004.

Nindos, A., J. Zhang, and H. Zhang, The magnetic helicity budget of solar active regions and coronal mass ejections, ApJ, 594, 1033-1048, 2003.

November, L.J., and G.W. Simon, Precise proper-motion measurement of solar granulation, ApJ, 333, 427-442, 1988.

Pariat, E., P. Démoulin, and M.A. Berger, Photospheric flux density of magnetic helicity, A&A, in press.

Pevtsov, A.A., R.C. Canfield, and T.R. Metcalf, Latitudinal variation of helicity of photospheric magnetic fields, ApJ, 440, L109-111, 1995.

Pevtsov, A.A., R.C. Canfield, and S.M. Latushko, Hemispheric helicity trend for solar cycle 23, ApJ, 549, L261-263, 2001.

Phillips, A.D., P.J. MacNeice, and S.K. Antiochos, The role of magnetic helicity in coronal mass ejections, ApJ, 624, L129-132, 2005.

Rust, D.M., Spawning and shedding helical magnetic fields in the solar atmosphere, GRL, 21, 241-244, 1994.

Rust, D.M., Magnetic helicity in solar filaments and coronal mass ejections, in *Physics of Magnetic Flux Ropes, Geophys. Monogr. Ser.*, vol. 111, edited by M.R. Brown, R.C. Canfield, and A.A. Pevtsov, pp. 221-227, AGU, Washington DC, 1999.

Seehafer, N., Electric current helicity in the solar atmosphere, Sol. Phys., 125, 219-232, 1990.

Sturrock, P.A., Maximum energy of semi-infinite magnetic field configurations, ApJ, 380, 655-659, 1991.

Taylor, J.B., Relaxation of toroidal plasma and generation of reverse magnetic fields, Phys. Rev. Lett., 33, 1139-1141, 1974.

Vourlidas, A., P. Subramanian, K.P. Dere, and R.A. Howard, Large-angle spectrometric coronagraph measurements of the energetics of coronal mass ejections, ApJ, 534, 456-467, 2000.

Welsch, B.T., G.H. Fisher, W.P. Abbett, and S. Regnier, ILCT: recovering photospheric velocities from magnetograms by combining the induction equation with local correlation tracking, ApJ, 610, 1148-1156, 2004

Wolfson, R., and B. Dlamini, Cross-field currents: An energy source for coronal mass ejections?, ApJ, 483, 961-971, 1997

Woltjer, L.A., A theorem on force-free magnetic fields, *Proc. Natl. Acad. Sci. USA,*, 44, 489, 1958.

Wu, S.T., W.P. Guo, D.J. Michels, L.F. Burlaga, MHD description of the dynamical relationships between a flux rope, streamer, coronal mass ejection, and magnetic cloud: An analysis of the January 1997 Sun-Earth connection event, JGR, 104, 14789-14802, 1999.

Zhang, H., Formation of current helicity and emerging magnetic flux in solar active regions, MNRAS, 326, 57-66, 2001.

Zhang, M., and B.C. Low, Magnetic flux emergence into the solar corona: III. the role of magnetic helicity conservation, ApJ, 584, 479-496, 2003.

Zhang, M., and B.C. Low Magnetic flux emergence into the solar corona. I. its role for the reversal of global coronal magnetic fields, ApJ, 561, 406-419, 2001.

Zhang, M., J.M. Stone, and B.C. Low, Formation of electric current sheets and magnetic flux ropes during magnetic flux emergence, AGU Fall meeting 2003, abstract SH42B-0517, 2003.

A. Nindos, Section of Astrogeophysics, Physics Department, University of Ioannina, Ioannina GR-45110, Greece (e-mail: anindos@cc.uoi.gr)

Figure 1. The evolution of a CME observed on June 2, 1998 with LASCO's C2 coronagraph.

Figure 1. The evolution of a CME observed on June 2, 1998 with LASCO's C2 coronagraph.

Figure 2. One–hour averages of the computed velocity vectors and the corresponding $G = -2\mathbf{u}\cdot\mathbf{A_p}B_n$ (gray–scale images) for active region 8375. The middle of each time interval is indicated in the panels. The maximum arrow length measures velocity of 0.7 km/sec. The full and dotted contours represent longitudinal magnetic field strengths of -200 and 200 G, respectively. The axis labels denote arcseconds on the solar photosphere (from Nindos et al. 2003).

Figure 2. One–hour averages of the computed velocity vectors and the corresponding $G = -2\mathbf{u}\cdot\mathbf{A_p}B_n$ (gray–scale images) for active region 8375. The middle of each time interval is indicated in the panels. The maximum arrow length measures velocity of 0.7 km/sec. The full and dotted contours represent longitudinal magnetic field strengths of -200 and 200 G, respectively. The axis labels denote arcseconds on the solar photosphere (from Nindos et al. 2003).

Figure 3. Contours of the stream function of an initial current-sheet magnetic field (left panel) and the final minimum-energy state of the field (right panel). The thick solid line in the current-sheet field shows the location of the current sheet (from Zhang & Low 2003).

Figure 3. Contours of the stream function of an initial current-sheet magnetic field (left panel) and the final minimum-energy state of the field (right panel). The thick solid line in the current-sheet field shows the location of the current sheet (from Zhang & Low 2003).

Figure 4. *Top*: Scatter plot of the pre-flare absolute values of α_{best} as a function of the flare's peak X-ray flux for active regions producing CME-associated flares. *Middle*: Same as top panel, but for the active regions producing flares that do not have associated CMEs. *Bottom*: Histograms of the values of α_{best} appearing in the top and middle panels. The solid line is the histogram of α_{best} of the active regions which give CME-associated flares and the dashed line is the histogram of α_{best} of the active regions which produce flares that do not have CMEs (from Nindos & Andrews 2004).

Figure 4. *Top*: Scatter plot of the pre-flare absolute values of α_{best} as a function of the flare's peak X-ray flux for active regions producing CME-associated flares. *Middle*: Same as top panel, but for the active regions producing flares that do not have associated CMEs. *Bottom*: Histograms of the values of α_{best} appearing in the top and middle panels. The solid line is the histogram of α_{best} of the active regions which give CME-associated flares and the dashed line is the histogram of α_{best} of the active regions which produce flares that do not have CMEs (from Nindos & Andrews 2004).

Figure 5. The absolute coronal helicity of the 78 ARs appearing in fig. 4. The format is identical to the format of fig. 4 (from Nindos & Andrews 2004).

Figure 5. The absolute coronal helicity of the 78 ARs appearing in fig. 4. The format is identical to the format of fig. 4 (from Nindos & Andrews 2004).

Plate 1. Helicity density evolution under the breakout model. The color map is altered for the last three frames to highlight the lower helicity densities in the expanding flux rope: in the first three frames the color scale represents helicity values from 0 to 2×10^{10} with a step of 1.052×10^9 while in the last three frames the color scale represents helicity values from 0 to 10^9 with a step of 5.263×10^7 (from MacNeice et al. 2004).

Plate 1. Helicity density evolution under the breakout model. The color map is altered for the last three frames to highlight the lower helicity densities in the expanding flux rope: in the first three frames the color scale represents helicity values from 0 to 2×10^{10} with a step of 1.052×10^9 while in the last three frames the color scale represents helicity values from 0 to 10^9 with a step of 5.263×10^7 (from MacNeice et al. 2004).

MAGNETIC HELICITY AND CMES

NINDOS

MAGNETIC HELICITY AND CMES

NINDOS

MAGNETIC HELICITY AND CMES

NINDOS

MAGNETIC HELICITY AND CMES

NINDOS

MAGNETIC HELICITY AND CMES

NINDOS

MAGNETIC HELICITY AND CMES

NINDOS

MAGNETIC HELICITY AND CMES

NINDOS

MAGNETIC HELICITY AND CMES

NINDOS

MAGNETIC HELICITY AND CMES

NINDOS

MAGNETIC HELICITY AND CMES

NINDOS

MAGNETIC HELICITY AND CMES

NINDOS

MAGNETIC HELICITY AND CMES

NINDOS

MAGNETIC HELICITY AND CMES

NINDOS

MAGNETIC HELICITY AND CMES

NINDOS

MAGNETIC HELICITY AND CMES

NINDOS

MAGNETIC HELICITY AND CMES

NINDOS

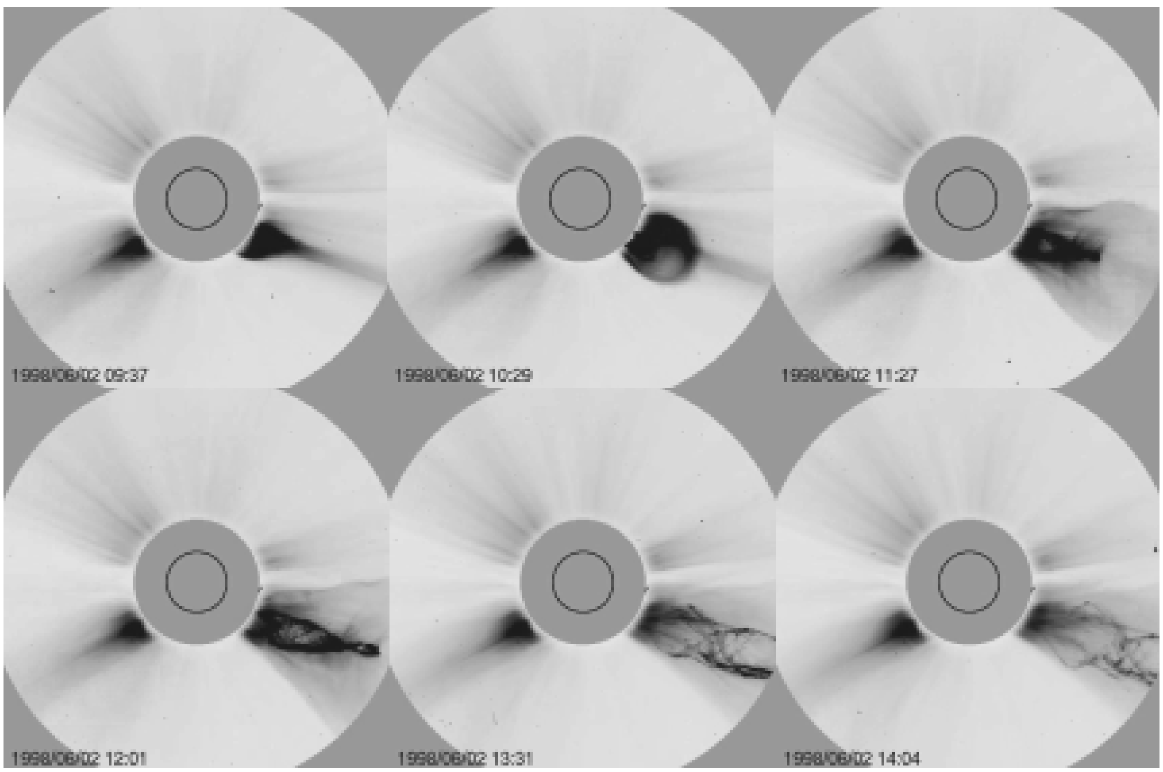
1998/06/02 09:37
1998/06/02 10:29
1998/06/02 11:27
1998/06/02 12:01
1998/06/02 13:31
1998/06/02 14:04

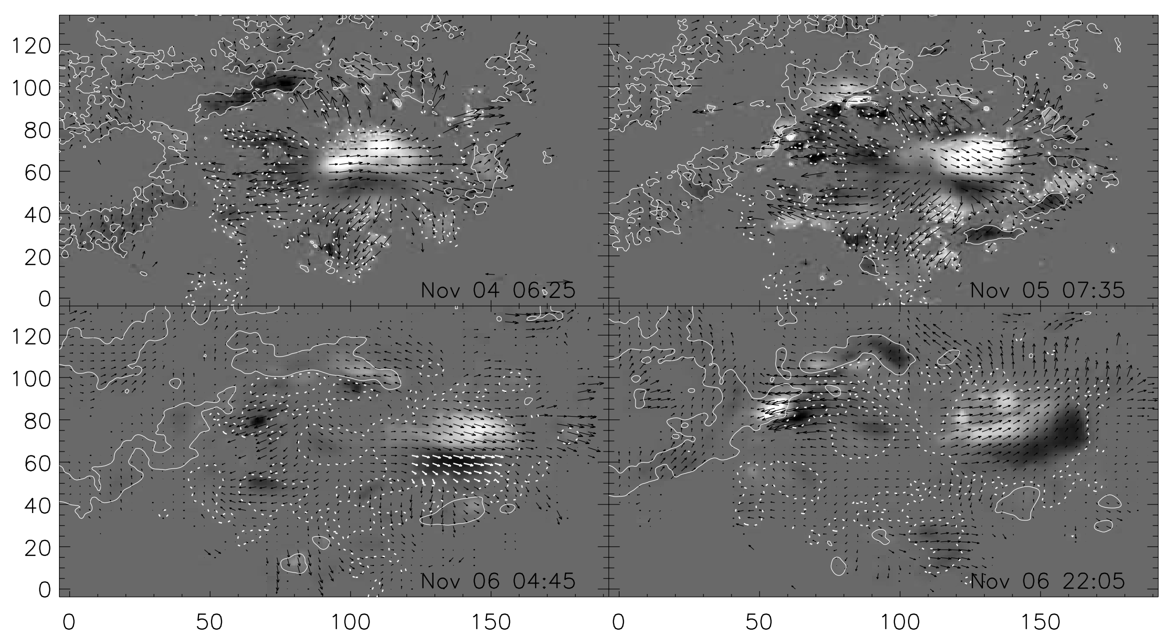

Nov 04 06:25
Nov 05 07:35
Nov 06 04:45
Nov 06 22:05
0
20
40
60
80
100
120
0
50
100
150

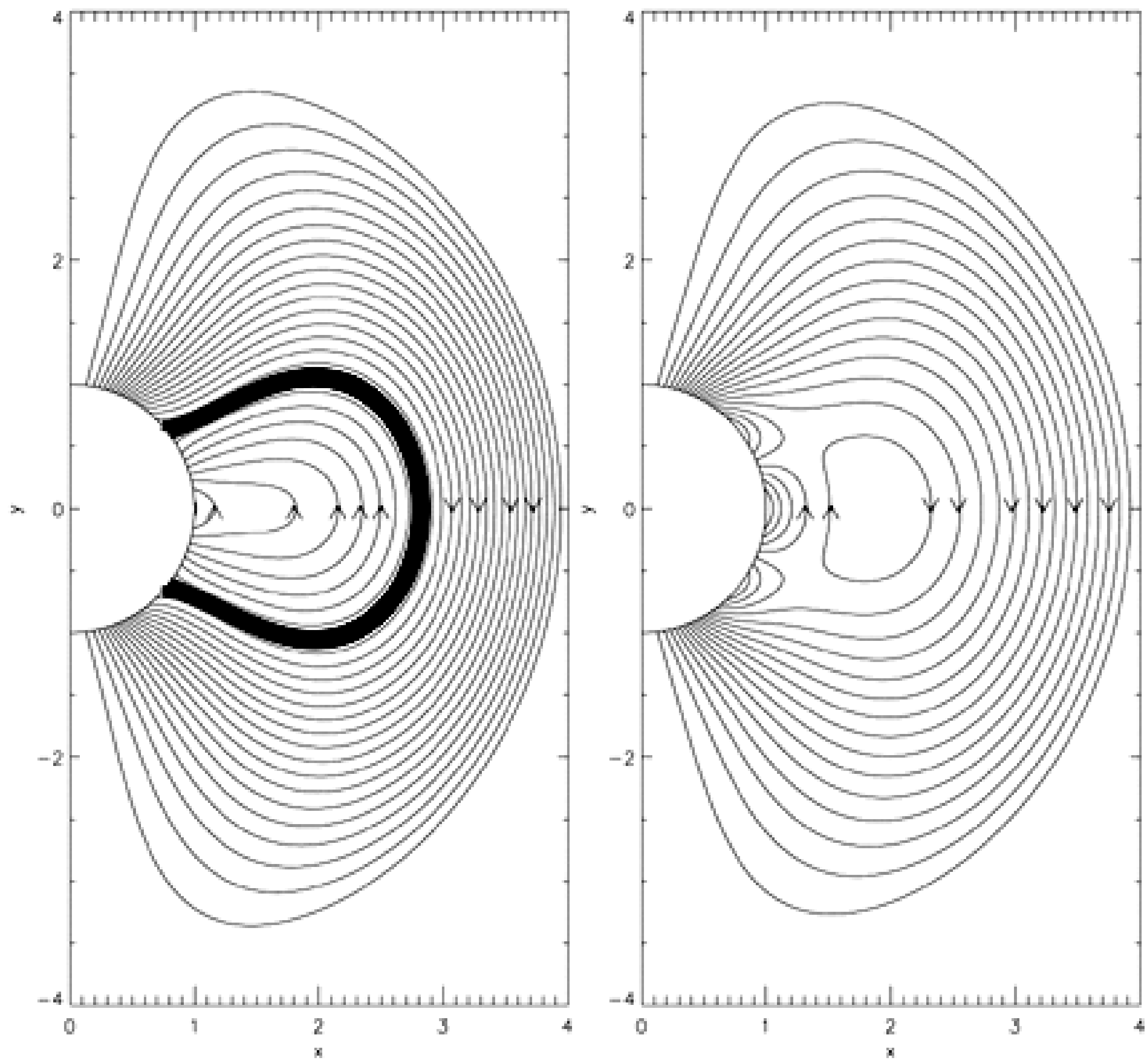

y
x
0
1
2
3
4
-4
-2

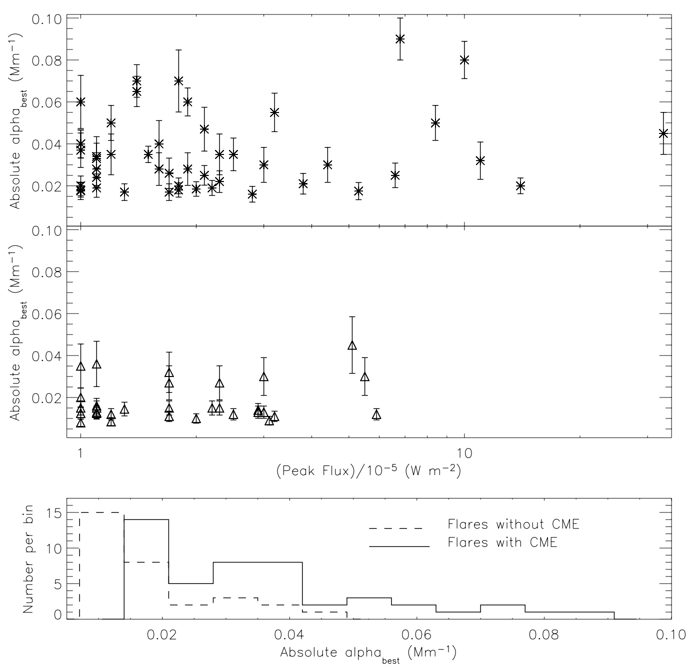

Absolute alpha$_{best}$ (Mm^{-1})
(Peak Flux)/10^{-5} (W m^{-2})
Number per bin
Flares without CME
Flares with CME

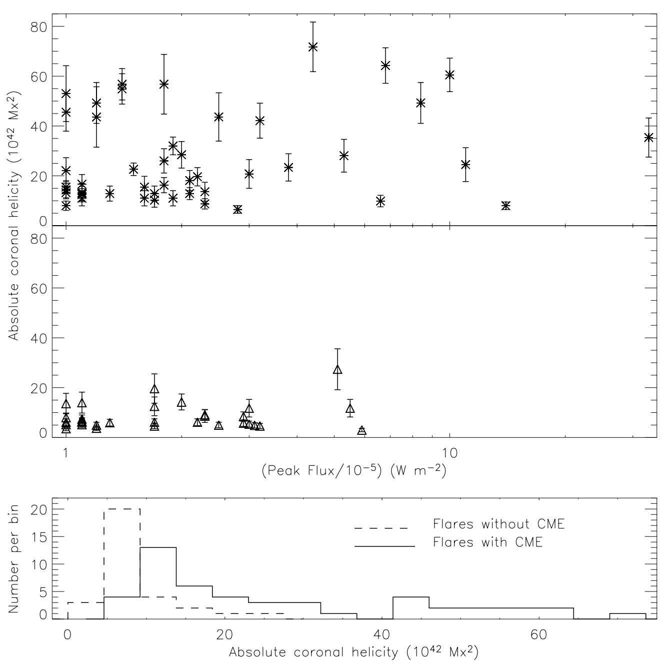

Absolute coronal helicity (10^42 Mx^2)
(Peak Flux/10^-5) (W m^-2)
Number per bin
Flares without CME
Flares with CME
Absolute coronal helicity (10^42 Mx^2)

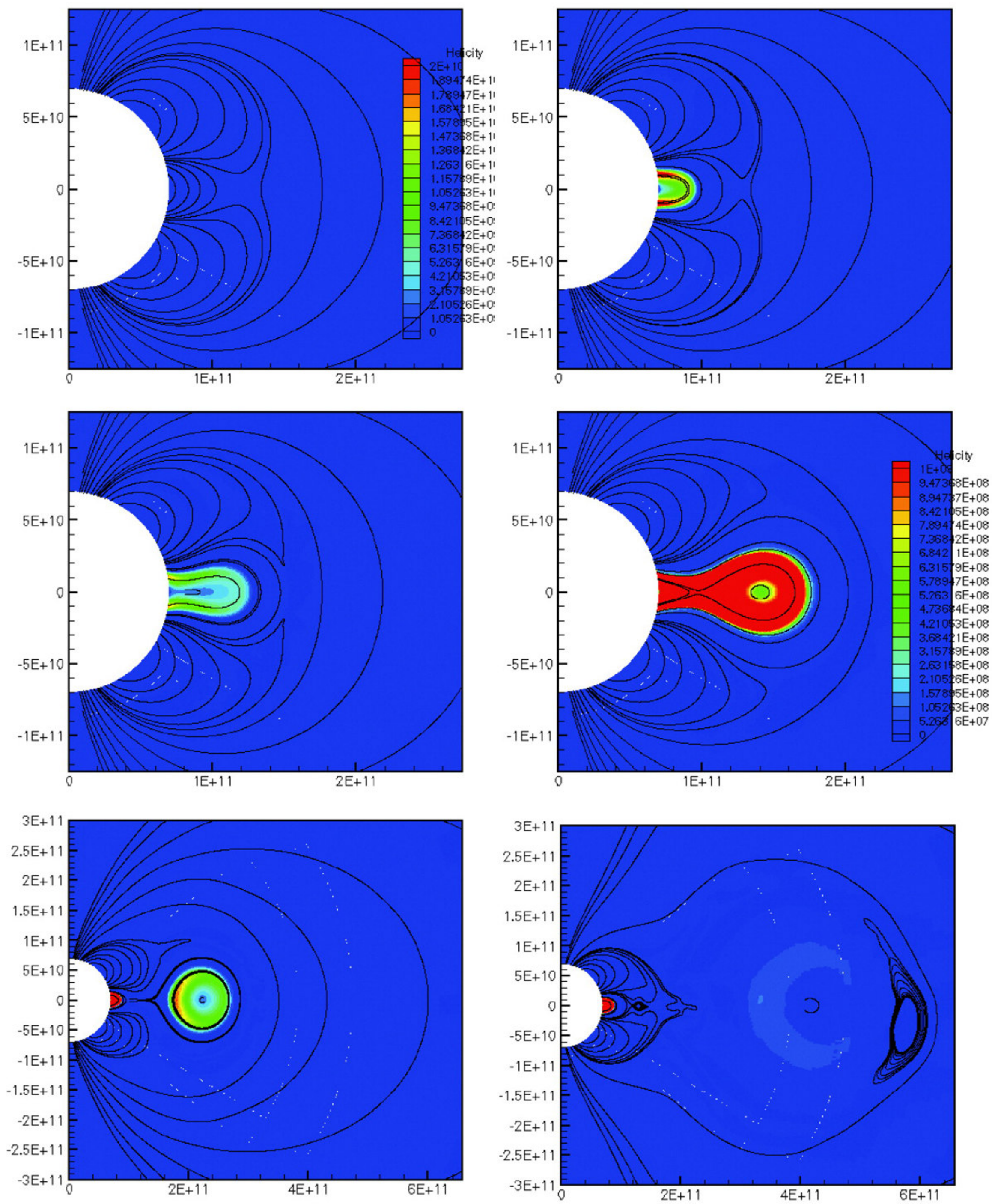
Helicity
1E+11
5E+10
0
-5E+10
-1E+11
1E+11
2E+11
3E+11
2.5E+11
2E+11
1.5E+11
-1.5E+11
-2E+11
-2.5E+11
-3E+11
4E+11
6E+11